19. Marhas, K. K. and Goswami, J. N., Boron isotopic composition in early solar system solids: An ion microprobe study. *Curr. Sci.*, 2000, **78**, 78–81.
20. Kallemeyn, G. W. *et al.*, Ordinary chondrites: Bulk compositions, classification, lithophile-element fractionations, and composition-petrographic type relationships. *Geochim. Cosmochim. Acta*, 1989, **53**, 2747–2767.
21. Ahrens, L. H., Si–Mg fractionation in chondrites. *Geochim. Cosmochim. Acta*, 1964, **28**, 411–423.
22. Eucken, A., Physikalisch-chemische Betrachtungen ueber die frueheste Entwicklungsgeschichte der Erde. *Nachr. Akad. Wiss. Goettingen, Math.-Phys. Kl.*, 2, 1944, 1–25.
23. Turekian, K. K. and Clark, S. P., Inhomogeneous accumulation of the earth from the primitive solar nebula. *Earth Planet. Sci. Lett.*, 1969, **6**, 346–348.
24. Vilas, F., Mercury: Absence of crystalline Fe^{2+} in the regolith. *Icarus*, 1985, **64**, 133–138.
25. Zellner, B. *et al.*, The E asteroids and the origin of the enstatite achondrites. *Geochim. Cosmochim. Acta*, 1977, **41**, 1759–1767.
26. Herndon, J. M., Total mass of ordinary chondrite material originally present in the Solar System. ArXiv: astro-ph/0410242, 2004.
27. Baedecker, P. A. and Wasson, J. T., Elemental fractionations among enstatite chondrites. *Geochim. Cosmochim. Acta*, 1975, **39**, 735–765.
28. Kallemeyn, G. W. and Wasson, J. T., The compositional composition of chondrites-I. The carbonaceous chondrite groups. *Geochim. Cosmochim. Acta*, 1981, **45**, 1217–1230.

Received 9 Febuary 2007; revised accepted 18 May 2007

Impact of Indonesian throughflow blockage on the Southern Indian Ocean

Vivek Kumar Pandey*, Vihang Bhatt, A. C. Pandey and I. M. L. Das

K. Banerjee Centre of Atmospheric and Ocean Studies, Institute of Inter-Disciplinary Studies, University of Allahabad, Allahabad 211 002, India

The present study deals with the numerical simulation of the Indonesian throughflow (ITF) via three major passages, namely Lombok strait (115°E, 8°S), Savu strait (122°E, 9°S) and Timor strait (128°E, 11°S), its seasonal variability and impact on the sea surface parameters due to its blockage. The model is initialized with the Levitus94 climatological dataset for annual mean temperature and salinity fields, and is forced by the seasonal and yearly varying da Silva SMD 1994 and Hellerman and Rosenstein wind datasets. The spin-up of the model has been carried out separately for open and closed Indonesian channels using both the surface wind climatologies. Numerical simulations confirm that the ITF is mainly towards Indian Ocean in a year. It has been observed that surface winds have an impact on the phase as well as magnitude of the ITF. The net effect of blockage is reduction in temperature of the Southern Indian Ocean and no significant change is seen in surface salinity.

Keywords: Blockage, Indonesian throughflow, passages, Southern Indian Ocean.

THE Indonesian throughflow (ITF) has long been a focus of research interest due to its impact on regional and global ocean circulation, both in modern and past time periods[1–3]. The ITF refers to the exchange of water and heat between the Indian Ocean (IO) and Pacific Ocean basins. It transfers warm, low-salinity waters from the western Pacific into the IO from where the Asian monsoon gathers strength. As an integral element of the global ocean circulation, it is influential in regulating climate and rainfall across Indonesia, India and Australia. The Indonesian Archipelago region has three major conduits for inter-ocean tropical thermocline water from the Pacific Ocean to the IO[4], namely Lombok strait (115°E, 8°S), Savu strait (122°E, 9°S) and Timor passage (128°E, 11°S).

The ITF is governed by Pacific Ocean to IO pressure gradient with strong seasonal and interannual variability[5,6]. The primary path of the ITF is through the Makassar strait[7,8]. The througflow is high during June–August (southeast monsoon) and low during December–February (northeast monsoon)[5]. During June–August, surface water is driven from Banda Sea into Floras, Java and South China seas, whereas during December–February, surface water from Java Sea and Makassar strait is driven across Floras Sea into Banda Sea[9]. Observations and model studies suggest that the ITF transport varies by as large as ±4 Sv (1 Sv = 10^6 m^3/s) with the phase of El Nino- Southern Oscillation (ENSO) (maximum ITF transport during La-Nina and minimum during El Nino)[10] and lags the ENSO cycle by 8–9 months[11].

In a unique study using a coupled ocean–atmosphere model, Schneider[12] has shown the effect of ITF on the oceanic circulation and thermocline depth in the IO and around Australia. This study shows that the ITF increases the surface temperature in the eastern IO. It also reduces surface temperatures in the equatorial Pacific Ocean and shifts the warm pool towards west, i.e. eastern IO. This self-control on the sea-surface temperature affects the atmospheric pressure in the entire tropics and mid-latitudes via atmospheric tele-connections. Numerical simulations also suggested that the ITF transport significantly contributes to the Eastern IO circulation[13]. The magnitude and variability of the Pacific and Indian Ocean (PACIO) throughflow for accurate determination of the mass, heat and salt fluxes in the PACIO region was also emphasized earlier[6,14,15]. Godfrey[16] discussed several aspects of ITF effects on the PACIO circulation and its impact on the surface heat flux of the IO.

The present study aims to carry out sensitivity studies with the Princeton Ocean Model (POM) to see the impact of ITF on the dynamics of the Southern Indian Ocean (SIO) and variability of the ITF.

*For correspondence. (e-mail: vivekkpandey@rediffmail.com)

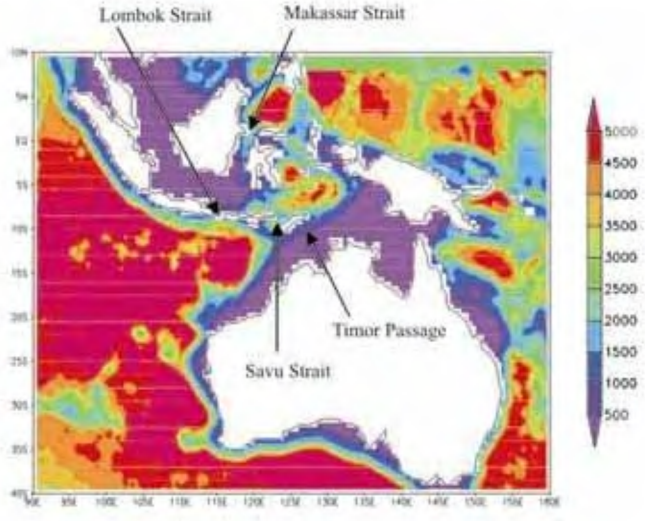

Figure 1. Topography and map of the study area used in the POM.

A three-dimensional primitive equation, sigma coordinate numerical ocean model POM[17,18] has been used to achieve the objectives. The model has been configured for the region of the Indonesian archipelago between 90°–160°E and 40°S–10°N (Figure 1). Figure 1 shows the topographic features around the Indonesian seas as well as three major passages, Lombook strait, Savu strait and Timor strait, having average depths of ~250, ~3000 and ~1500 m respectively. A curvilinear orthogonal system with a fixed resolution of 0.5° × 0.5° has been used as horizontal model grid in the model and staggered, Arakawa C-grid type of finite difference scheme has been used for numerical implementation. The vertical grid was fragmented in the 14 sigma layers with higher resolution in the upper mixed layer and lower resolution in the deep ocean. The vertical mixing coefficients were provided by the turbulence scheme[19]. The horizontal mixing coefficients for momentum (viscosity) and tracers (diffusivity) were calculated by a Smagorinsky-type formulation[20].

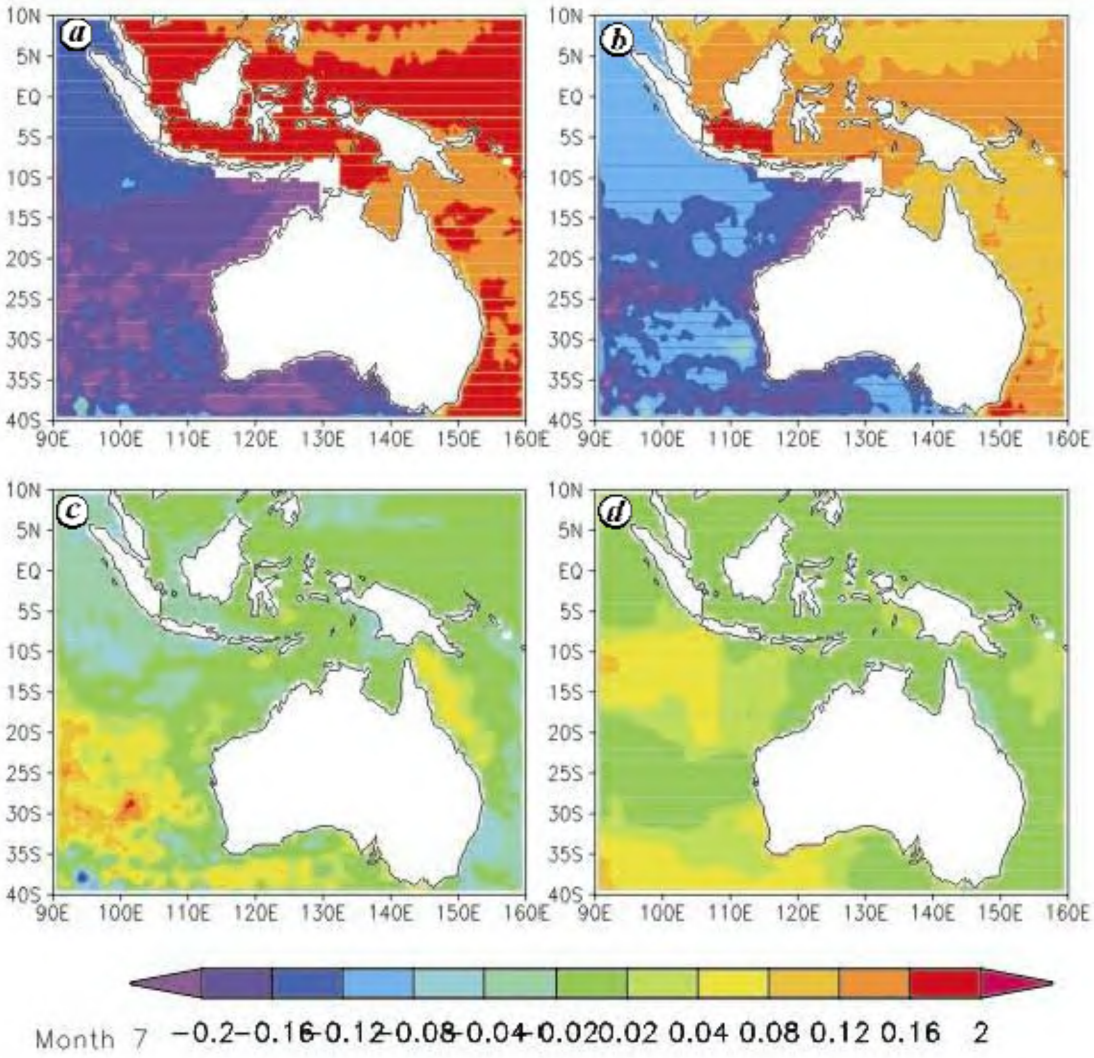

Figure 2. ***a***, Difference in surface elevation (closed-open) for July when forced with Hellerman wind stress climatology. ***b***, Same as (***a***) but model forced with da Silva wind stress climatology data. ***c***, Difference in surface elevation when forced with different wind stress climatologies (Hellerman–da Silva). ***d***, Difference in wind stress climatology for July (Hellerman–da Silva).

In the sigma coordinate system, the number of levels is the same everywhere in the ocean, irrespective of the depth of the water column. It is, therefore, possible to resolve the bottom boundary layer wherever needed and hence is best suited for shallow coastal regions[21]. The model integration has been carried out for 10 years for the domain shown in Figure 1. The numerical experiment has been carried out to study the impact of blockage of Indonesian channels on the SIO dynamics. Initially, the model was spun from the cold-start for open as well as blocked Indonesian channels using climatological wind stress data available from Hellerman and Rosenstein[22], and da Silva *et al.*[23]. Apart from forcing data, the model was initialized using climatological temperature and salinity data obtained from Levitus *et al.*[24], and Levitus and Boyer[25] for spin-up of the model from cold-start. The Hellerman wind stress data available at $2° \times 2°$, and temperature and salinity data at $1° \times 1°$ available from Levitus climatology were brought to model grid resolution of $0.5° \times 0.5°$ using bilinear interpolation. The da Silva wind stress climatologies were available at the model grid resolution. On the expiry of the spin-up period of the model, simulation results–output were stored every month for one more year using the same climatological wind stress data. The sensitivity of the model simulations to wind stress data used to drive the model has also been studied.

Thereafter, model integration has been carried out for one more year using the above-mentioned climatologies, and simulations were stored every month. The difference plots for the surface elevations (blocked-open) have been shown for July (Figure 2) and December (Figure 3). It can be observed that the surface elevation for July was

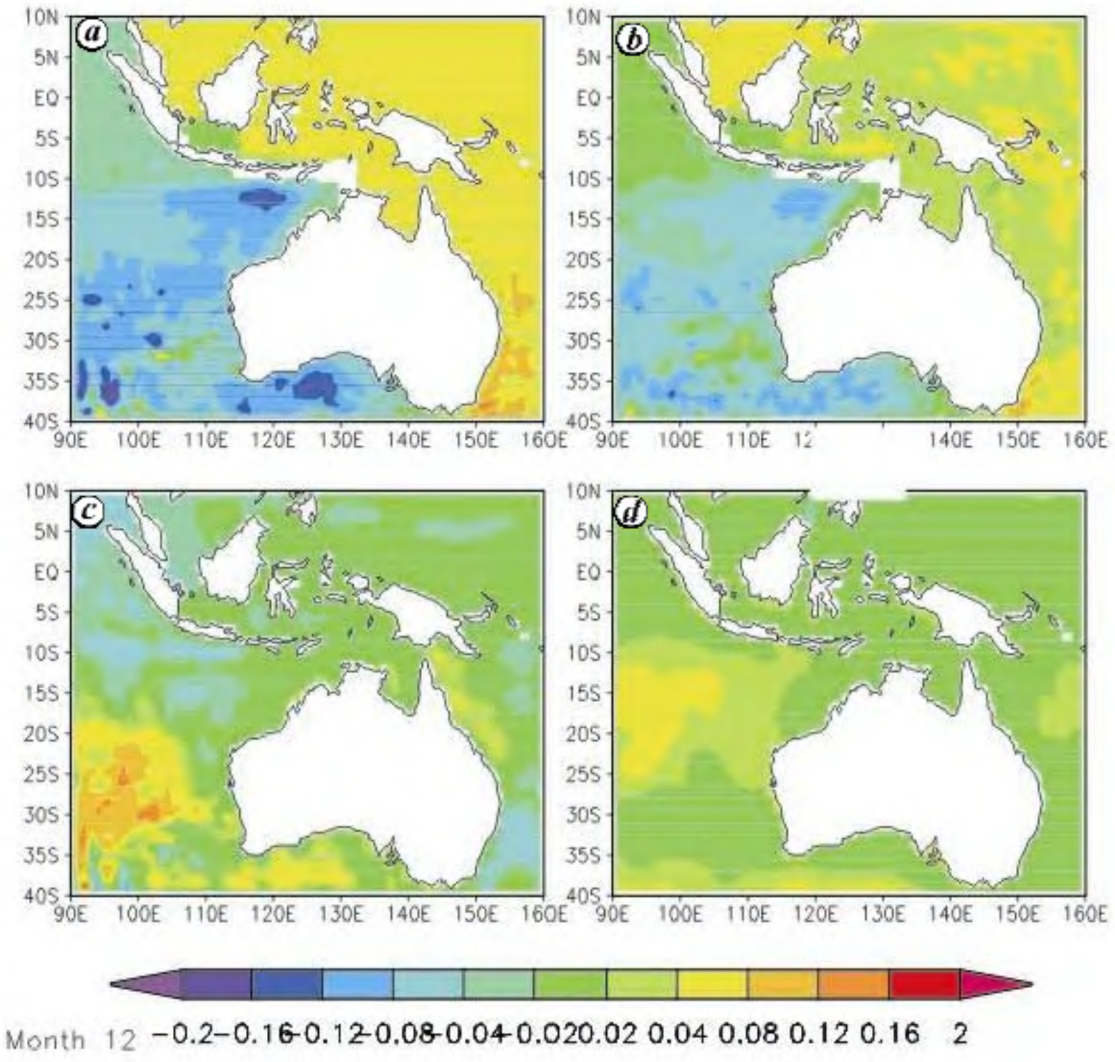

Figure 3. ***a***, Difference in surface elevation (closed-open) for December when forced with Hellerman wind stress climatology. ***b***, Same as (***a***) but model forced with da Silva wind stress climatology data. ***c***, Difference in surface elevation when forced with different wind stress climatologies (Hellerman–da Silva). ***d***, Difference in wind stress climatology for December (Hellerman–da Silva).

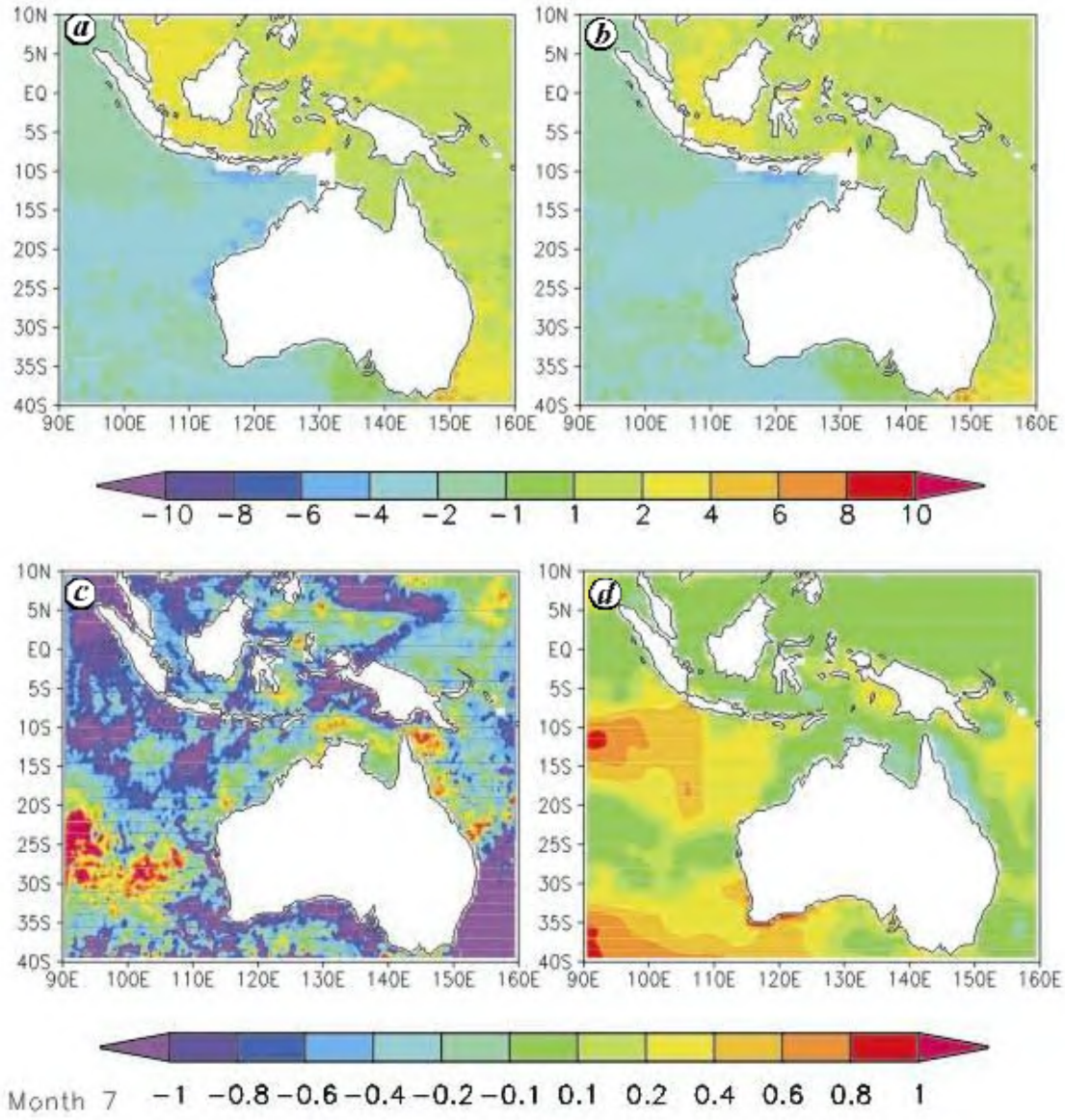

Figure 4. ***a***, Difference in sea surface temperature (closed-open) for July when forced with Hellerman wind stress climatology. ***b***, Same as (***a***) but model forced with da Silva wind stress climatology data. ***c***, Difference in sea surface temperature when forced with different wind stress climatologies (Hellerman–da Silva). ***d***, Difference in wind stress climatology for July (Hellerman–da Silva).

reduced by more than 0.16 m in the SIO, whereas it increased by the same amount in the Pacific Ocean for model simulations using both wind stress climatologies. Java Sea exhibits higher surface elevations (>0.16 m) when forced with da Silva wind stress climatology (Figure 2 *b*). In December, surface elevation in the Pacific Ocean increased by a marginal amount of 0.04–0.08 m and decreased by 0.16 m or more in some regions of the SIO due to blockage of the Indonesian channels (Figure 3 *a*). Similar results were obtained for the model simulations using da Silva wind stress climatology (Figure 3 *b*). The difference plot of surface elevations (Hellerman and Rosenstein–da Silva) for July (Figure 2 *c*) and December (Figure 3 *c*) shows that the model simulated surface elevations are higher in the SIO, in general, when Hellerman wind stress data were used to force the model. However, these differences are uncorrelated with those in the wind stress data (Figures 2 *d* and 3 *d*). Model simulations using Hellerman wind stress climatology for July indicate that the SIO gets cooler by 2–6°C, whereas the Pacific Ocean gets warmer by 2–4°C due to the blockage of the Indonesian channels (Figure 4 *a*). It has also been observed that the rise in temperature of this order was observed in the Java Sea, South China Sea and some parts of the Banda Sea, whereas cooling of the order of 4–6°C was observed in Savu Sea. The difference plot of surface temperature

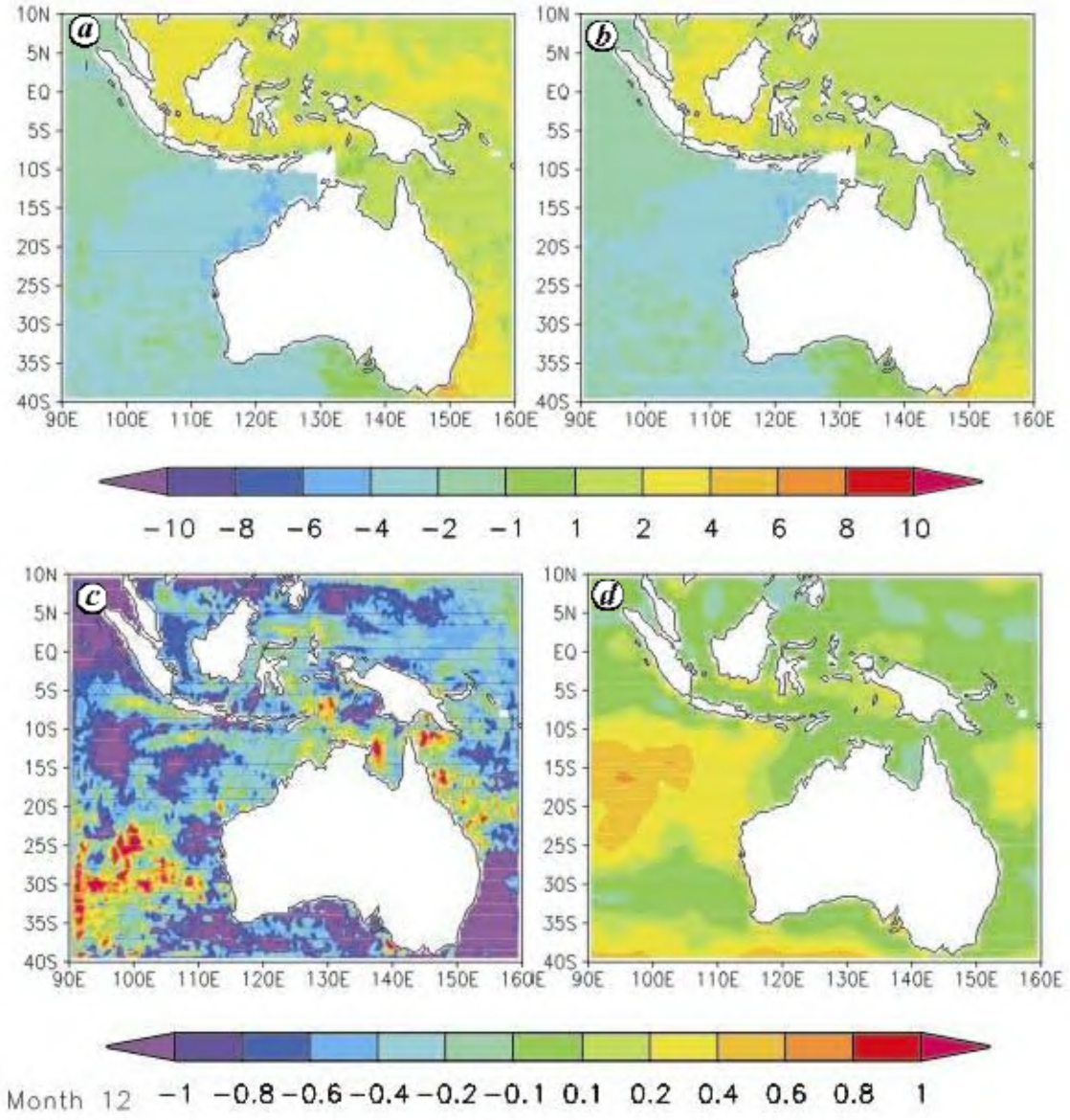

Figure 5. ***a***, Difference in sea surface temperature (closed-open) for December when forced with Hellerman wind stress climatology. ***b***, Same as (***a***) but model forced with da Silva wind stress climatology data. ***c***, Difference in sea surface temperature when forced with different wind stress climatologies (Hellerman–da Silva). ***d***, Difference in wind stress climatology for December (Hellerman–da Silva).

(Figure 4 *a*) also indicates surface warming (>4°C) near the eastern Australian coast due to channel blockage. Model simulations using da Silva wind stress also show warming of surface temperature in the Pacific Ocean by 1–2°C, whereas only Java Sea shows an increase in temperature more than 2°C. This difference plot for December (Figure 5 *a* and *b*) also exhibits similar temperature difference as observed in July, when forced with Hellerman and da Silva wind stress climatologies. The general warming of the Pacific Ocean and cooling of the IO can be explained using the fact that the heat transport (nearly 0.6 PW; 1 PW = 10^{15} W) between the Pacific Ocean and the IO is cut-off[26]. Recently, Gordon *et al.*[27] have concluded that the ITF is far cooler than estimated earlier, based on ocean current and temperature. Temperature and ocean current time series obtained for this region for any duration can be utilized to calculate heat transport of the ITF[28] and consequently its influence on the SIO. There are results that support model studies that the ITF heat, derived from the Pacific Ocean, is ultimately lost to the atmosphere in the SIO[29]. The ENSO variability in the internal energy transport is calculated on the basis of long-term mooring observational data of temperature[30]. Warming in the Pacific Ocean is consistent with the eastward tendency of horizontal velocity, which turns poleward near the eastern tropical Pacific advecting warmer waters

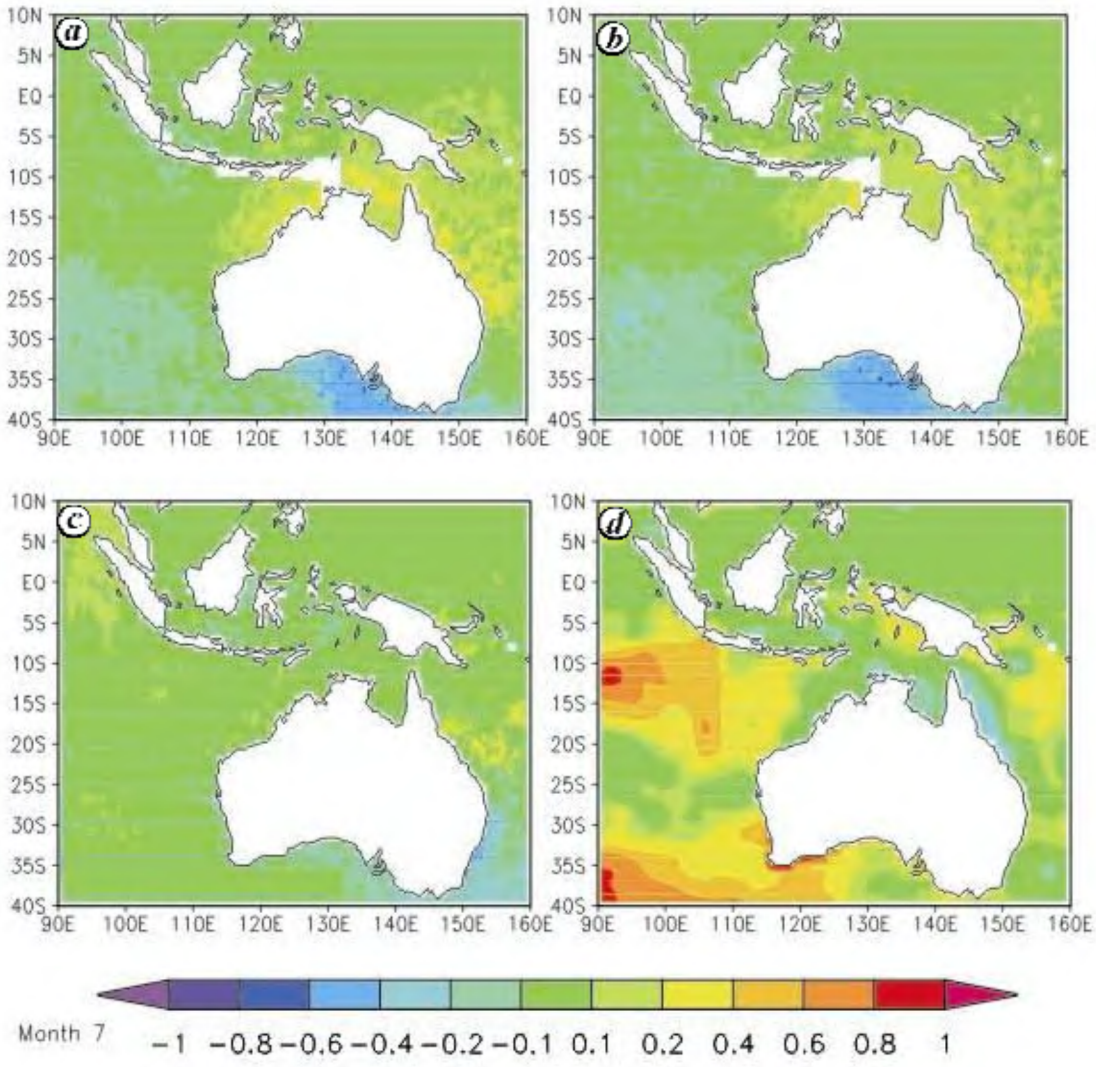

Figure 6. ***a***, Difference in sea surface salinity (open-closed) for July when forced with Hellerman wind stress climatology. ***b***, Same as (***a***) but model forced with da Silva wind stress climatology data. ***c***, Difference in sea surface salinity when forced with different wind stress climatologies (Hellerman–da Silva). ***d***, Difference in wind stress climatology for July (Hellerman–da Silva).

in the western Pacific towards the east and spreading them poleward in the eastern Pacific. The difference plot of surface temperature (Hellerman–da Silva) shows higher surface temperatures in SIO and lower surface temperature in some parts of South Pacific (Figures 4 *c* and 5 *c*). In this case also difference in the temperature is uncorrelated with difference in the wind stress used to force the model. The impact of blockage of Indonesian channels on surface salinity remains more or less unaffected. Maximum hike in surface salinity was observed in the South Australian Sea by an amount of 0.6‰, whereas it was lowered by order of 0.1–0.4‰ in the Timor Sea. Figures 6 and 7 show changes in surface salinity due to difference in surface forcing for July and December respectively. It appears from the figures that surface salinity is less sensitive to surface wind forcing. The volume transports through individual channels and net volume transport through PACIO are shown in Figure 8 *a* (using Hellerman wind stress data) and Figure 8 *b* (using da Silva wind stress data). Time series of volume transport (Figure 8 *a*) indicates that maximum volume transport from the Pacific Ocean to IO is from Savu strait (~6/5 Sv), followed by Timor passage (~3.5/2 Sv) and Lombook strait (~2/1.75 Sv). This gives a gross volume transport of ~10/9 Sv, when Hellerman/da Silva wind stress data were used to force the model. Maximum volume transport from the Pacific Ocean to the IO was observed during June–September, i.e. southeast monsoon period. Model simulation suggests that during the northeast monsoon, the ITF reverses its direction, i.e. transport occurs from the IO to the Pacific Ocean. This reversal of the throughflow has also been simulated with varying magnitude each year in different modelling studies[31]. Model simulations using both wind stress data indicate the gross

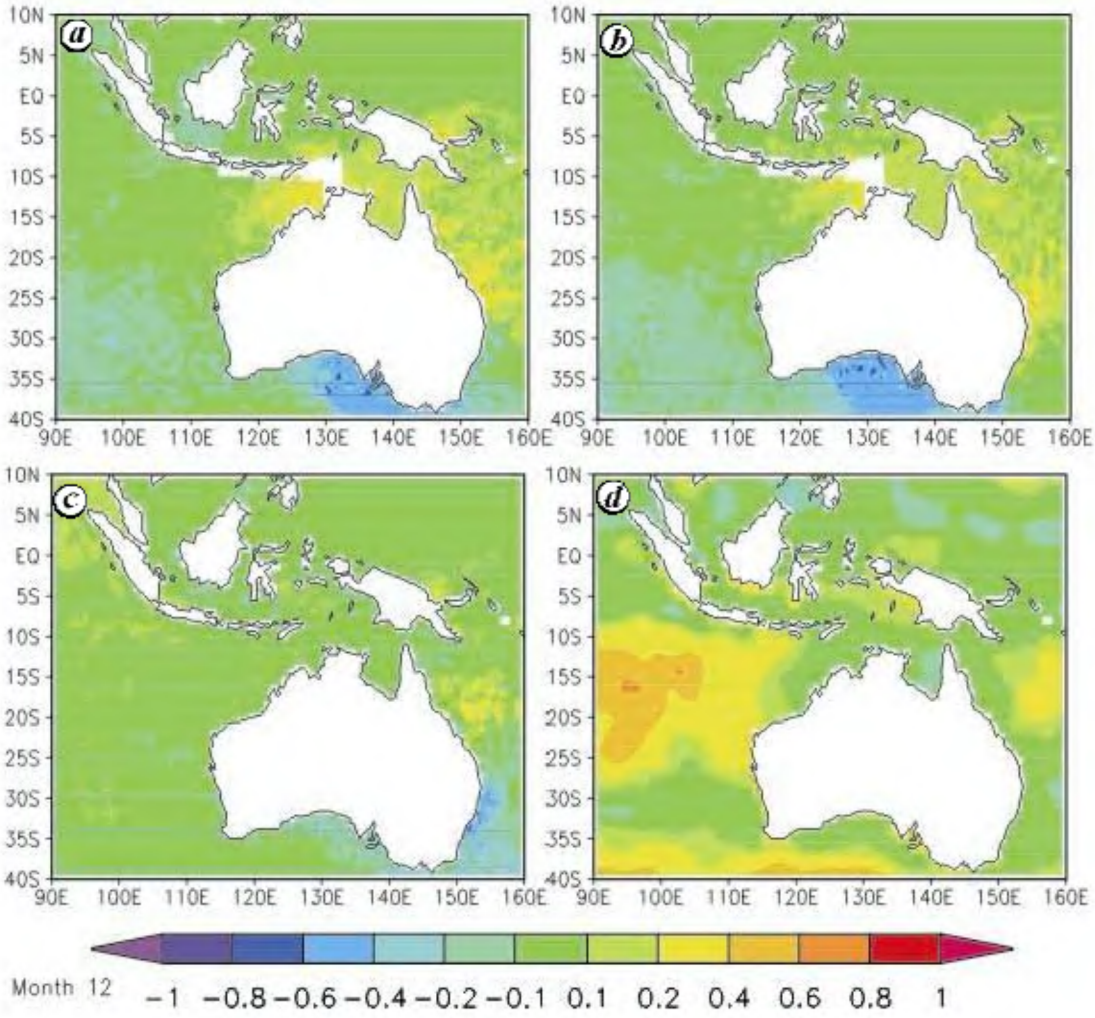

Figure 7. ***a***, Difference in sea surface salinity (open-closed) for December when forced with Hellerman wind stress climatology. ***b***, Same as (***a***) but model forced with da Silva wind stress climatology data. ***c***, Difference in sea surface salinity when forced with different wind stress climatologies (Hellerman–da Silva). ***d***, Difference in wind stress climatology for December (Hellerman–da Silva).

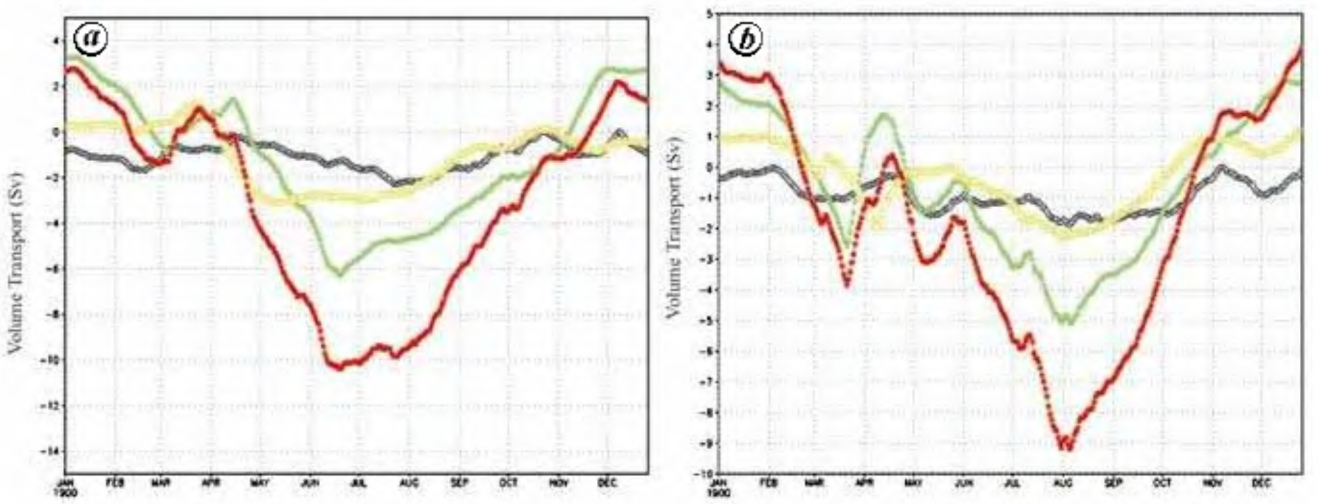

Figure 8. Time series of model-computed volume transport from Lombook strait (black line), Savu strait (green line) and Timor passage (yellow line) and net volume transport from PACIO (red line) when forced with (***a***) Hellerman winds and (***b***) da Silva winds.

volume transport of ~3 Sv through PACIO from the IO to the Pacific Ocean. However, peaking of the westward transport (Pacific Ocean to IO) occurs in June and thereafter remains nearly constant up to August, when Hellerman wind stress data were used to force the model, whereas a peak of the westward transport was observed in August for the da Silva wind stress as surface forcing.

POM has been used to investigate the ITF and its impact on the SIO dynamics. Sensitivity experiments have also been carried out to investigate the impact of topographic features on model simulation. It can be concluded that smoothening of the topography increases the zonal and meridional integrated volume transport through the Indonesian region. This change in transport influences the heat budget of the SIO. It has been observed in this study that higher volume transport tends to increase the surface temperature, surface elevation and hence the dynamic height of the sea surface.

The blockage of throughflow channels has shown a significant impact on the SIO. It can be concluded from the study that blockage of the Indonesian channels results in significant changes in the surface temperature in the SIO as well as the Pacific Ocean. It is also evident from study that the blockage of the channels causes 4°C cooling in the SIO and 2°C warming of the western Pacific Ocean. It has also been observed that surface wind forcing has an impact on the model simulation, as a result of sensitivity experiments of wind effect on ocean. However, the sensitivity study also suggests that there is no correlation with the spatial distribution of the difference between the two wind climatologies.

1. Srinivasan, M. S. and Sinha, D. K., Early Pliocene closing of the Indonesian seaway: Evidence from northeast Indian Ocean and southwest Pacific deep sea cores. *J. Southeast Asian Earth Sci.*, 1998, **16**, 29–44.
2. Srinivasan, M. S. and Sinha, D. K., Ocean circulation changes in the Indo-Pacific during 5.6 to 4.2 Ma: Planktic foraminiferal and isotopic evidences. *Proc. Indian Acad. Sci. (Earth Planet. Sci.)*, 2000, **109**, 315–328.
3. Cane, M. A. and Molnar, P., Closing of the Indonesian seaway as a precursor to the east African aridification around 3–4 million years ago. *Nature*, 2001, **411**, 157–162.
4. Gordon, A. L., Interocean exchange of thermocline water. *J. Geophys. Res.*, 1986, **91**, 5037–5047.
5. Wyrtki, K., Indonesian throughflow and associated pressure gradient. *J. Geophys. Res.*, 1987, **92**, 12941–12946.
6. Kindle, J. C., Hurlburt, H. E. and Metzger, E. J., On the seasonal and interannual variability of the Pacific–Indian Ocean throughflow. In Western Pacific International Meeting and Workshop on TOGA-CORE (eds Picaut, J., Lukas, R. and Decroix, T.), ORSTOM, New Caldonia, France, 1989, pp. 355–366.
7. Ffield, A. and Gordan, A. L., Vertical mixing in the Indonesian thermocline. *J. Phys. Oceanogr.*, 1992, **22**, 184–195.
8. Gordon, A. L., Susanto, R. D. and Ffield, A., Throughflow within Makassar Strait. *Geophys. Res. Lett.*, 1999, **26**, 3325–3328.
9. Gordon, A. L. and Ffield, A., Thermocline of the Floras and Banda Sea. *J. Geophys. Res.*, 1994, **99**, 18235–18242.
10. Mayers, G., Variation of Indonesian throughflow and El Nino-Southern Oscillation. *J. Geophys. Res.*, 1996, **101**, 12255–12263.
11. England, M. H. and Huang, F., On the interannual variability of the Indonesian throughflow and its linkage with ENSO. *J. Climate*, 2005, **18**, 1435–1444.
12. Schneider, N., Indonesian throughflow and the global climate system. *J. Climate*, 1988, **11**, 676–689.
13. Wajsowicz, R. C., Interannual variations in the Indo-Pacific throughflow forced by ECMWF wind-stress anomalies for 1985–1989. In *Toga Notes*, Nova Southern University Press, Florida, 1994, vol. 15, pp. 6–11.
14. Piola, A. R. and Gordon, A. L., Pacific and Indian upper layer salinity budget. *J. Phys. Oceanogr.*, 1984, **14**, 747–753.
15. Toole, J. M., Problems of interbasin exchanges and marginal sea overflows. *Bull. Am. Meteorol. Soc.*, 1987, **68**, 136–140.
16. Godfrey, J. S., The effects of the Indonesian throughflow on ocean circulation and heat exchange with the atmosphere: A review. *J. Geophys. Res.*, 1996, **101**, 12217–12237.
17. Blumberg, A. F. and Mellor, G. L., A description of a three-dimensional coastal ocean circulation model. In *Three Dimensional Coastal Ocean Models* (ed. Heaps, N. S.), AGU, Washington DC, 1987, vol. 4, p. 208.
18. Mellor, G. L., In *Users Guide for a Three-Dimensional, Primitive Equation, Numerical Ocean Model*, Princeton University, Princeton, NJ, 2004, p. 56.
19. Mellor, G. L. and Yamada, T., Development of a turbulent closure model for geophysical fluid problems. *Rev. Geophys.*, 1982, **20**, 851–875.
20. Smagorinsky, J., Manabe, S. and Holloway, J. L., Numerical results from a nine-level general circulation model of the atmosphere. *Mon. Weather Rev.*, 1965, **93**, 727–768.
21. Kantha, L. and Clayson, C. A., In *Numerical Models of Oceans and Oceanic Processes*, Academic Press, 2000, p. 940.
22. Hellerman, S. and Rosentein, Normal monthly wind stress over the world ocean with error estimates. *J. Phys. Oceanogr.*, 1983, **13**, 1093–1104.
23. da Silva, A., Young, A. C. and Levitus, S., In *Atlas of Surface Marine Data, NOAA, Atlas NESDIS*, 1994, vol. 6, p. 83.
24. Levitus, S., Buugett, R. and Boyer, T. P., In *World Ocean Atlas 1994, Salinity, NOAA Atlas NESDIS*, 1994, vol. 3, p. 99.
25. Levitus, S. and Boyer, T. P., In *World Ocean Atlas 1994, Temperature, NOAA Atlas NESDIS*, 1994, vol. 4, p. 11.
26. Verschell, M. A., Kindle, J. C. and O'Brien, J. J., Effects of Indo-Pacific througflow on the upper tropical Pacific and Indian oceans. *J. Geophys. Res.*, 1995, **100**, 18409–18420.
27. Gordon, A. L., Dwi, R. and Vranes, K., Cool Indonesian throughflow as a consequence of restricted surface layer flow. *Nature*, 2003, **425**, 824–828.
28. Pandey, V. K. and Pandey, A. C., Heat transport throughflow: Indonesian throughflow. *J. Indian Geophys. Union*, 2006, **10**, 273–277.
29. Vranes, K., Gordon, A. L. and Ffield, A., The heat transport of the Indonesian throughflow and implications for Indian Ocean heat budget. *Deep-Sea Res.*, 2002, **49**, 1391–1410.
30. Ffield, A., Vranes, K., Gordon, A. L., Susanto, R. D. and Garzoli, S. L., Temperature variability within the Makassar Strait. *Geophys. Res. Lett.*, 2000, **27**, 237–240.
31. Lee, T., Fukumori, I., Menemenlis, D., Xing, Z. and Fu, L. L., Effects of the Indonesian throughflow on the Pacific and Indian Oceans. *J. Phys. Oceanogr.*, 2002, **32**, 1404–1429.

ACKNOWLEDGEMENTS. We thank Dr Tal Ezer, Princeton University, Princeton and Dr P. C. Pandey for their valuable suggestions. We thank NCAOR, GOA/DOD for financial assistance through a research project.

Received 26 July 2006; revised accepted 15 March 2007